Available online at www.sciencedirect.com
SCIENCE DIRECT®
Polymer 45 (2004) 3175–3184
polymer
www.elsevier.com/locate/polymer

Interface structure of photonic multilayers prepared by plasma enhanced chemical vapor deposition

Hyeonjae Kim[a,*], Mark D. Foster[a,*], Hao Jiang[b,c], Scott Tullis[b], Timothy J. Bunning[b], Charles F. Majkrzak[d]

[a]*Maurice Morton Institute of Polymer Science, The University of Akron, 170 University Ave., Akron, OH 443253909, USA*
[b]*Air Force Research Laboratory, Materials and Manufacturing Directorate, Wright-Patterson Air Force Base, OH 54533, USA*
[c]*Anteon Co., Dayton, OH 45431, USA*
[d]*NIST Center for Neutron Research, Gaithersburg, MD 20899, USA*

Received 26 January 2004; received in revised form 5 March 2004; accepted 8 March 2004

Abstract

The structures of substrate/layer, layer/layer, and layer/air interfaces in optical multilayers made using plasma enhanced chemical vapor deposition (PECVD) have been probed for the first time using X-ray reflectivity and neutron reflectivity. From the point of view of optical applications the interfaces are extremely sharp, sharper than is often achievable with the self-assembly of block copolymers or deposition techniques in which the polymer layers contact while in a fluid state. The average interface width, a_I, between layers made from different precursors is about 40 Å (16 Å rms). The layer/layer interfaces are generally 2–3 times broader than the layer/air interfaces. Polymeric fluorocarbon films deposited on a Si substrate using PECVD with octafluorocyclobutane (OFCB) monomer show uniform scattering length density with depth except for a region of molecular thickness immediately adjacent to the substrate. Films made from deuterated benzene show uniform density throughout the film thickness.

Keywords: PECVD multilayer; Interface structure; Reflectivity

1. Introduction

Single layer, multilayer, and graded refractive index films for photonic applications may all in principle be fashioned from organic monomers using plasma enhanced chemical vapor deposition (PECVD) [1]. Plasma polymerized materials offer several advantages over organic layers deposited by other means, including good adhesion to substrates, solvent-free processing, smooth and pinhole-free structure, and long-term chemical, thermal and environmental stability [2].

Key to further exploiting the advantages offered by PECVD processing is the determination of details of the layer structures and structure of interfaces between layers. Because the chemistry of plasma polymerized films is so complex, considerable effort has been expended to elucidate the chemical composition and chemical structure of PECVD films [3–14] using various analytical techniques such as FT-IR, XPS, and UV–VIS absorption spectroscopy. The study of the films' physical structure or morphology has been limited, generally, to investigations of thickness and topography or roughness at the surface using techniques such as ellipsometry [3], and AFM [3,4,11,15–17]. Ellipsometry is also used extensively to investigate the optical properties of the films [3,12,14,15,18,19]. Foerch and coworkers [20] have used surface plasmon spectroscopy to study changes in the structure of plasma-polymerized films of allylamine with exposure to solution environments. As yet few studies of interface structure in PECVD polymer films have been reported. The interface structure is of interest from both practical and fundamental points of view. Practically the interface structure affects optical properties and dictates adhesion at the interface. Of fundamental interest is the question of how the crosslinking that occurs in the PECVD process influences the formation of a polymer/polymer interface. At interfaces between ordered domains of block copolymers [21–24] or between immiscible

* Corresponding authors. Tel.: +1-3309725390; fax: +1-3309725290.
E-mail addresses: hkim1@uakron.edu (H. Kim), mfoster@uakron.edu (M.D. Foster).

0032-3861/$ - see front matter © 2004 Elsevier Ltd. All rights reserved.
doi:10.1016/j.polymer.2004.03.028

polymer pairs [25–29] the interface width reflects the outcome of a competition between entropic and enthalpic factors. Interface widths in such systems may be specified in terms of σ, with σ being the standard deviation of the interface position in the direction perpendicular to the surface (z), or may be specified in terms of a_I defined as

$$a_I = \frac{(\phi^A - \phi^B)}{(\partial\phi(z)/\partial z)_{\phi=(\phi^A+\phi^B)/2}} \quad (1)$$

where ϕ^A and ϕ^B denote the compositions of the two phases away from the interface. a_I is the same as $\sqrt{2\pi}\,\sigma$ and values of a_I in the range of 30–80 Å have been reported for ordered block copolymers [21–24] and immiscible blends [25–29]. These interface widths are measured in a way that incorporates broadening by capillary waves [27,29,30] that are present at fluid interfaces.

There have been some studies of the structure of PECVD films made from other monomer structures using scattering techniques [31–33]. The structures of amorphous carbon films prepared by PECVD from hydrogen and methane precursors have been probed by neutron reflectivity [31]. The measured reflectivity was analyzed with a two-layer model in which it was assumed that a diamond-like carbon layer of approximately 30 Å was present at the air interface. Those authors obtained values of composition, density, thickness and roughness of each layer. Bontempi et al. [32] studied the growth process of silicon–nitrogen alloys deposited on Si substrates by PECVD using X-ray reflectivity. They were able to determine structural parameters of the films such as thickness, density and roughness in the cases of both stoichiometric and non-stoichiometric films. A 10–15 Å thick oxidized layer with a lower density was observed at the air interface.

It would be highly advantageous to have detailed information on the structure of the PECVD films interfaces, not only the interfaces with the substrate and air, but also those between layers in multilayer films. The complementary techniques of X-ray and neutron reflectivity are uniquely suited to simultaneously providing precise, non-destructive characterization of all of these interfaces, and have been used widely in the characterization of other sorts of polymer interfaces [34–40]. In the current contribution they have been used to probe the structure of layers made from benzene (B), deuterated benzene (dB), or OFCB precursors. Plasma-polymerized B (PP-B) and plasma-polymerized dB (PP-dB) have comparatively high refractive indices ($n = 1.61$ and 1.62 at 500 nm, respectively) while plasma-polymerized OFCB (PP-OFCB) serves as the low refractive index film ($n = 1.40$ at 500 nm). The molecular structure, thickness of the film, surface roughness, and detailed structure of the interfaces of thin films of single species and multilayer films of alternating layers of PP-OFCB and PP-dB have been quantified in the measurements described below. Even though there have been several investigations [3–7,9,10,14] with PECVD films of these precursors or analogous precursors, detailed structural information such as the interface width between adjacent layers in a multilayer is reported here for the first time.

2. Experimental section

2.1. Sample preparation

While the structure of multilayer films is the ultimate interest of this project, a series of films, including single layer films from each precursor, a bilayer film, and a multilayer film of 5 dB/OFCB bilayers, was investigated to systematically gather structural information. A 'bilayer' film of two layers will be denoted as an 'A/B bilayer', where A is the abbreviation for the precursor of the layer closer to the substrate. Likewise a multilayer film of two components will be denoted as an 'A/B multilayer', with A being the abbreviation for the precursor of the layer closer to the substrate.

Principles of the CVD set-up and deposition method have been published elsewhere [41]. Briefly, the flowing afterglow reaction system used for plasma polymerization of the samples was essentially the same as that described previously [14]. The vacuum in the 10 cm diameter glass reactor was maintained at 0.5–2 Torr, while 50–200 standard cm^3/min of 99.999% argon was flowed directly through capacitively coupled electrode plates, with a primary radio frequency discharge at 13.56 MHz.

HPLC grade B (C_6H_6) with purity of 99.9%, supplied by Aldrich Co. [42] or dB (C_6D_6) with purity of 99.5%, supplied by Cambridge Isotope Laboratories Inc. [42] was used as the high-refractive index monomer. The B or dB reservoir was maintained at 19.0 ± 0.1 °C by a thermostatted water bath to keep the vapor pressure constant. The other monomer, OFCB (C_4F_8), supplied by SynQuest Laboratories Inc. [42] as compressed gas with purity of >99%, was used as the low refractive index precursor. These monomers were used as received without further purification.

Either the B (or dB) vapor or OFCB gas was introduced into the chamber 7 cm downstream from the plasma zone. The flow rate of the B vapor was controlled in the range of 0.004–0.5 cm^3/min and that of dB vapor was controlled in the range of 0.004–0.3 cm^3/min by a manually adjusted high-accuracy metering-valve. The flow rate of the OFCB gas was 0.5–5 cm^3/min, controlled by a Sierra 902C flow-controller [42]. The 2″ or 3″ diameter silicon wafer substrate for the film deposition was placed 1–3 cm further downstream from the monomer inlet. For the preparation of films of more than one layer, the precursor materials were introduced sequentially into the chamber as needed.

2.2. X-ray and neutron reflectivities

X-ray reflectometry (XR) [37,43] and neutron reflectometry (NR) [43] are useful for characterizing the structures

of thin films in the direction perpendicular to the surface. They are unique techniques to probe interfacial structures 'buried' inside the film. In reflectometry the ratio of specularly reflected to incident intensity for a flat, thin film is measured over a range of incident angles to yield a reflectivity curve. From this curve can be inferred information about the film thickness and microroughnesses at the air/film interface, the interface with the substrate, and interfaces inside the film if they exist. A reflectometry experiment is sensitive to variations in structure in the direction normal to the surface because the scattering vector, q, lies normal to the surface. X-ray reflectometry is specifically sensitive to differences in the electron densities, ρ_e, which are related to the atomic numbers of the constituent elements and mass density. These differences in electron density may alternatively be described using the real part of the refractive index for X-rays, δ, or X-ray scattering length density (SLD), $(b/V)_x$, both of which are proportional to electron density:

$$\delta = \frac{\lambda^2}{2\pi}\left(\frac{b}{V}\right)_x \tag{2}$$

$$\left(\frac{b}{V}\right)_x = r_e\rho_e \tag{3}$$

$$\rho_e = \frac{N_A\rho_b\sum b_i}{MW}, \quad b_i = Z_i, \tag{4}$$

where λ is the wavelength, b is total scattering length in the scattering volume V, r_e is the classical electron radius, N_A is Avogadro's number, ρ_b is mass density, Σb_i is the total scattering length in a representative 'structural unit' and is given by the sum of the atomic numbers (Z_i) of the atoms in that structural unit, and MW is the molecular weight of this structural unit. On the other hand, NR is sensitive to variations in the *neutron* SLD, $(b/V)_n$. While X-ray scattering length varies in a monotonic fashion through the periodic table, neutron scattering lengths of the elements do not and elements or isotopes that differ very little in atomic number may have strongly different scattering lengths. Thus contrast for NR can be greatly enhanced by deuterium labeling due to the widely different scattering lengths of hydrogen and deuterium. So NR may be sensitive to structures that cannot be readily probed by XR or vice versa. In this contribution we take advantage of this complementarity.

XR was measured using a spectrometer [44] mounted on a rotating anode source [45] (Rigaku, 12 kW RU200) [42] with Cu K_α radiation ($\lambda = 1.54$ Å) or at the beamline 1-BM [46] ($\lambda = 1.26$ Å) at the advanced photon source synchrotron. Reciprocal space resolutions δq_z in both instances are about 0.001 $Å^{-1}$. To correct the experimentally measured specular reflection intensity, the background scattering was estimated by performing longitudinal diffuse scans in which the detector and incident angles were increased simultaneously, but with the incident angle offset by 0.1 or 0.07° from the specular condition. This background intensity was then subtracted from the experimentally measured specular intensity.

NR was measured on the NG1 reflectometer at the National Institute of Standards and Technology (NIST) Center for Neutron Research using a wavelength of 4.75 Å. Reflectivities were collected with approximately constant relative resolution in q ($\delta q/q \approx 0.02$) by increasing the sizes of the collimating and detector slits with increasing incident angle. This approach takes best advantage of the intensity available at larger values of q. Variation in the resolution function with incident angle was considered in the data fitting by appropriate convolution of the model reflectivity with a Gaussian resolution function.

The structure of a thin film cannot be obtained by directly inverting the reflectivity data, due to the loss of phase information [37,43]. Instead, a candidate model is assumed for the film structure and the parameters of the model varied until a simulated reflectivity curve calculated for the model structure using the Parratt formalism [47] agrees sufficiently well with the experimental data. In the model the variation in the refractive index, $n(z)$ through an interface between two adjacent homogeneous layers j and $j+1$ is described by an error function with interface roughness σ_j

$$n(z) = \frac{n_j + n_{j+1}}{2} - \frac{n_j - n_{j+1}}{2}\,\mathrm{erf}\left(\frac{z - z_j}{\sqrt{2}\sigma_j}\right). \tag{5}$$

NR and XR data are analyzed analogously. Small differences in the film thicknesses measured with the two techniques probably derive from the fact that the films are slightly thinner at their edges than in the center, due to hydrodynamic effects that occur for the larger samples required for reflectivity analysis. Both XR and NR capture global descriptions of film structure, averaging laterally over mm^2 to cm^2, depending on the beam footprint, which varies with the instrument used. The footprint width is constant with q and equal to 1 mm for the synchrotron XR measurements, 10 mm for XR measurements with the rotating anode, and 25 mm for the NR measurements. The length of the footprint exceeds the sample size at the smallest q for all types of measurements and decreases with increasing q for a given instrument. The minimum footprint length (at $q = 0.5$ $Å^{-1}$) was 6 mm for synchrotron measurements, 5 mm for rotating anode measurements, and 29 mm for NR measurements. While the same samples were characterized with the two techniques, the locations studied on a given sample were not identical for XR and NR. Ellipsometry measurements revealed that the film close to the edge of the substrate, which might be excluded from the XR measurements over most of the q range due to the smaller footprint, is typically about 3% thinner than the film in the center of the substrate.

3. Results and discussion

3.1. Interface structure of single layer films

The structure was first determined for a single layer of PP-OFCB. The NR data are shown in Fig. 1 along with the best model fit and the corresponding model $(b/V)_n$ profile. The corresponding model parameters obtained by both NR and XR are summarized in Table 1. At the beginning of the study the mass density of the PP-OFCB film was unknown, so it was not possible to calculate *a priori* a value of $(b/V)_n$ for the film. However, because the value of $(b/V)_n$ is higher for the film than for the substrate, $(b/V)_n$ for the film can be determined from the location of the critical edge in the reflectivity curve. The mass density of the film can then be calculated [48,49] to be 1.9 ± 0.08 g/cm^3, given [14] that the ratio of fluorine to carbon, F/C, is 1.8, using the equation,

$$(b/V)_n = \frac{N_A \rho_b \sum b_i}{MW} \tag{6}$$

where, Σb_i is the sum of neutron scattering lengths in a representative 'structural unit', $CF_{1.8}$, of the plasma polymerized polymer. The determination of this film's mass density is interesting, since this density is difficult to obtain otherwise.

Once the mass density of the film has been determined by NR, the X-ray refractive index of the material can be determined using the following relation with the known value of the composition,

$$n = 1 - \delta + i\beta, \tag{7}$$

where δ is the dispersion term as is defined in Eq. (2) and β is the absorption term and can be formulated as

$$\beta = \frac{\lambda}{4\pi}\mu, \tag{8}$$

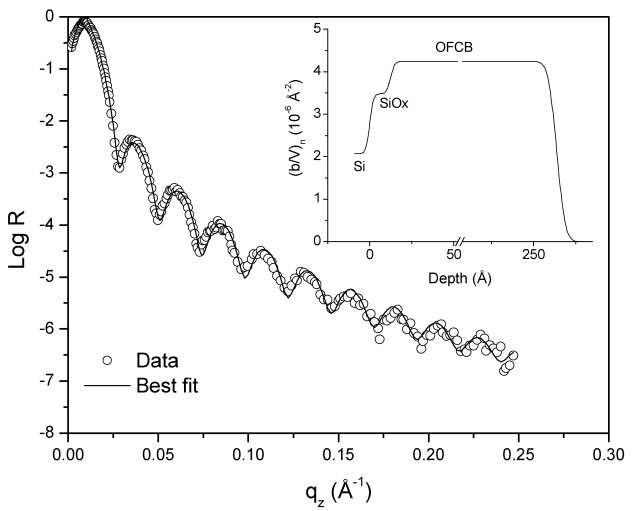

Fig. 1. Neutron reflectivity (NR) data (circles) for the PP-OFCB single layer film and the best fit model reflectivity (solid line) obtained with the model $(b/V)_n$ profile shown in the inset. Zero on the depth scale is taken as the center of the interface between the Si substrate and its oxide layer.

Table 1
Summary of structure model parameter values for single layer films

Layer	Parameter	PP-OFCB		PP-dB	
		NR	XR	NR	XR
SiO_x	d (Å)[a]	12	11	14	8
Interface	σ (Å)[a]	2	3	8	3
Transition	d (Å)	NA	6	NA	NA
Interface	σ (Å)	NA	4	NA	NA
OFCB or dB	d (Å)	251	256	238	249
Interface	σ (Å)	4	5	5	5

[a] Uncertainty in d is ±2 Å and that of σ inferred from the fitting process is 15–20%.

where μ is the linear absorption coefficient. While depth profiles derived from X-ray reflectivity data are often plotted as δ vs. depth, in this paper we plot instead the quantity $(b/V)_x$ due to the obvious analogy to the quantity $(b/V)_n$ we use to describe the depth profiles obtained from NR. Conversion between δ and $(b/V)_x$ is readily done using Eq. (2).

The complementarity of the XR and NR measurements is highlighted by the analysis of the XR data for the PP-OFCB single layer film compared in Fig. 2 with simulated reflectivity curves for two candidate models. A model envisioning uniform $(b/V)_x$ through the entire film thickness is not able to properly capture the variation in fringe amplitude with scattering vector, as is shown in Fig. 2(a). Only after all attempts to reconcile the data with such a model failed was additional complexity introduced into the

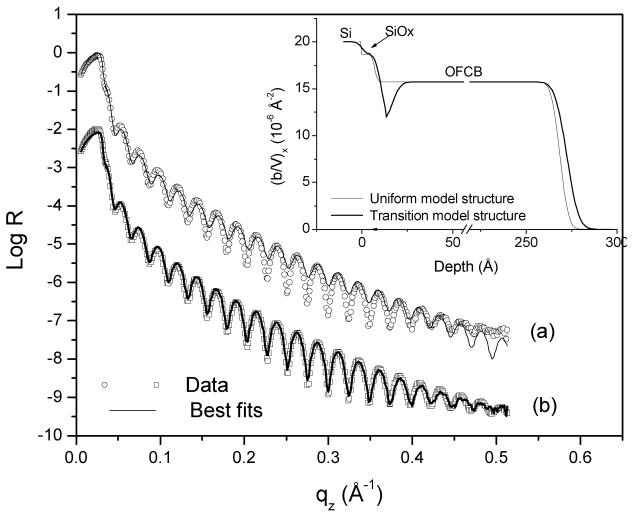

Fig. 2. A single X-ray reflectivity (XR) data set (open symbols) for the PP-OFCB single layer film compared with the simulated reflectivities from two different candidate model structures represented in the inset. The structures are described by $(b/V)_x$, which is proportional to electron density. (a) XR data compared with the best fit obtained with a uniform density model structure. The uniform layer model cannot account for the fringe amplitudes. (b) XR data compared with the best fit obtained with a structure model accounting for a low density region adjacent to the substrate. For clarity, these data and the corresponding best fit have been shifted by two orders of magnitude from curve (a).

structure model for the film. The oxygen and nitrogen contents in the PP-OFCB film are negligible (less than 1%) [14]. Therefore, one can exclude the possibility that there is an oxidized layer with lower density at the air surface [32]. One can also exclude the possibility that there is an internal layer containing significant percentages of any elements other than carbon and fluorine. However, adding to the model a transition region of molecular dimension (6 Å) immediately adjacent to the substrate, as shown in the inset of Fig. 2, allows one to fit the data well, as shown in Fig. 2(b). Why do the profiles measured by NR and XR differ? If the region of low $(b/V)_x$ had the same F/C ratio (= 1.8) as does the rest of the film, a dip should also have appeared in the $(b/V)_n$ profile derived from the NR data. No dip is seen in the $(b/V)_n$ profile. Thus, the composition at the interface with the substrate is different from that in the bulk. Therefore, a 'dip' shows up in the $(b/V)_x$ profile, but not in $(b/V)_n$ profile. It has been reported [3–5,14] that species of different F/C ratio can exist in the PP-OFCB structure, resulting in the 'average' structural unit of the polymer having a composition of $CF_{1.8}$ [14]. The reactivity of the CF species with the surface is greater [50] than the reactivities of the CF_2 and CF_3 species and the reactivity of the CF species with the substrate may differ from that of the CF species with the other species. It is also conceivable that the more negatively charged CF_3 and CF_2 species are more strongly repelled from the negatively charged SiO_x surface than is the CF species. If the substrate selectively reacts with the CF species there will be a region in which the CF species is dominant near the substrate. In this case, the $(b/V)_n$ in the transition region could be the same as that in the bulk with the mass density of the region slightly lower than that in the bulk, i.e. $\rho_{tr} \approx 1.8$ g/cm^3. Then the $(b/V)_x$ of the transition region would be much lower than that of the bulk.

NR data and the best model fit for a PP-dB single layer film are shown in Fig. 3, with the corresponding model $(b/V)_n$ profile in the inset. There are some advantages in using deuterated benzene instead of 'regular' benzene even though the $(b/V)_n$ contrasts for the dB/OFCB and B/OFCB pairs are about the same. First, incoherent scattering is reduced by using dB, since the incoherent scattering from deuterium is much lower than that from hydrogen. Secondly, one is able to obtain the $(b/V)_n$ of the film unambiguously when using dB because the critical angle of the film is higher than that of the substrate. The surface of the PP-dB film is as smooth as that of the PP-OFCB film. While the NR curves for the PP-dB and PP-OFCB films are qualitatively very similar, the XR curve for the PP-dB film, shown in Fig. 4, looks very different from that of the PP-OFCB film. The amplitudes of the fringes in the XR curve plotted on a linear-log scale initially increase as q_z increases for the PP-OFCB film, while the amplitudes of the fringes decrease somewhat with increasing q_z at higher q_z for the PP-dB film.

It is more difficult to analyze the XR data of the PP-dB film because not much is known yet from other techniques about the composition of the PP-dB material. Even though $(b/V)_n$ of the PP-dB film has been determined by NR, the material composition must be known to calculate the exact value of mass density of the film. However, self-consistently analyzing XR and NR data from several samples made it possible to determine the composition of the PP-dB layer to within a small uncertainty. The composition, expressed in terms of an average compositional unit CD_x, was first assumed to lie in the range of $CD_{0.7}$ to $CD_{1.5}$ (These are not the exact chemical formulae. The key issue is the D/C ratio). The material density of the film was calculated for possible candidate compositions within this range using Eq. (6). A constant oxygen content of 3 atomic% was assumed whatever the D/C ratio considered [14]. Then the XR data for the PP-dB single layer film were fit using the various possible compositions in this range and the corresponding

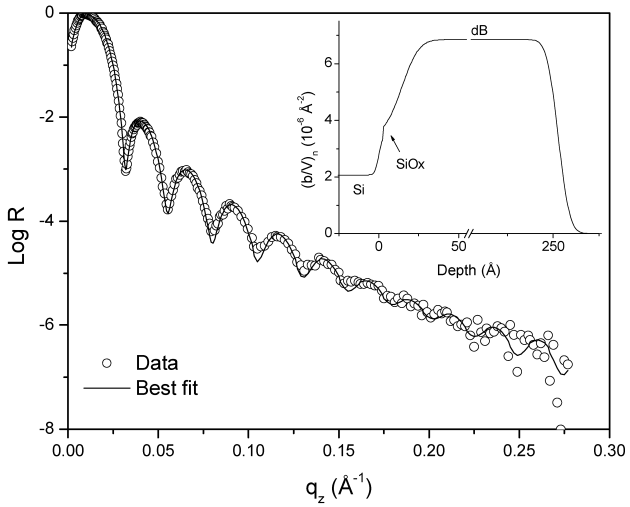

Fig. 3. NR data (open symbols) and the best fit obtained with a model structure shown in the inset for a PP-dB single layer film. The model structure is described in terms of $(b/V)_n$ as a function of depth of the film.

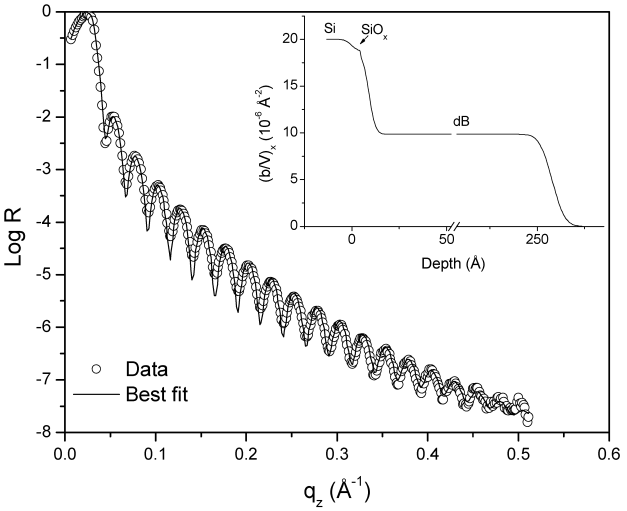

Fig. 4. XR data for a PP-dB single layer film measured with a laboratory Cu K_α source and the best fit obtained with a model structure shown in the inset.

calculated densities of the PP-dB film. The best results were obtained for compositions between $CD_{1.15}$ and $CD_{1.32}$. Then the NR and XR data for the bilayer and multilayer films were fit using compositions in this more narrowly defined range and corresponding densities of the layers. The quality of fit obtained using different sets of parameters was similar for compositions between $CD_{1.15}$ and $CD_{1.32}$. However, the best results were obtained with the composition $CD_{1.23}$ and the results shown in the remainder of the paper were all obtained with that composition. Plasma polymerization is a complex process and its chemistry less well understood than that of conventional polymerization reactions. However, it seems reasonable to have a higher D/C ratio in the film than in the precursor itself. If benzene radicals were primarily incorporated into the polymer one would expect a composition of CD_x with $x < 1$. The deuterium radicals are more reactive than the benzene radicals so a higher ratio of D is incorporated than would be if only benzene radicals were incorporated in the structure. Using the composition of $CD_{1.23}$ one obtains good agreement between the model fit and the measured reflectivity for the single layer of PP-dB without adding any special features in the density profile such as the transition region found for the PP-OFCB film.

The structure of the PP-OFCB film indicated by XR data measured at The University of Akron and the NR data measured at NIST is confirmed by the analysis of separate XR measurements at the 1-BM beamline at the Advanced Photon Source. XR data from three single layer films of PP-B and three single layers of PP-OFCB are shown in Fig. 5. The thicknesses range from 67 to 652 Å for PP-B and 50 to 290 Å for PP-OFCB. The thicknesses of the PP-B films were estimated by fringe spacings and those of the PP-OFCB films were obtained by detailed data fitting. The best fit of each PP-OFCB film data set is superposed on that data set. Fits to the XR curves of the PP-B films are not presented because the 'bulk' densities of the films are unknown. The densities of the films cannot be unambiguously determined by NR because the critical angle of the film is smaller than that of the substrate. However, the qualitative character of the XR data from the single layer PP-B films is the same as that of the data from the single layer PP-dB films.

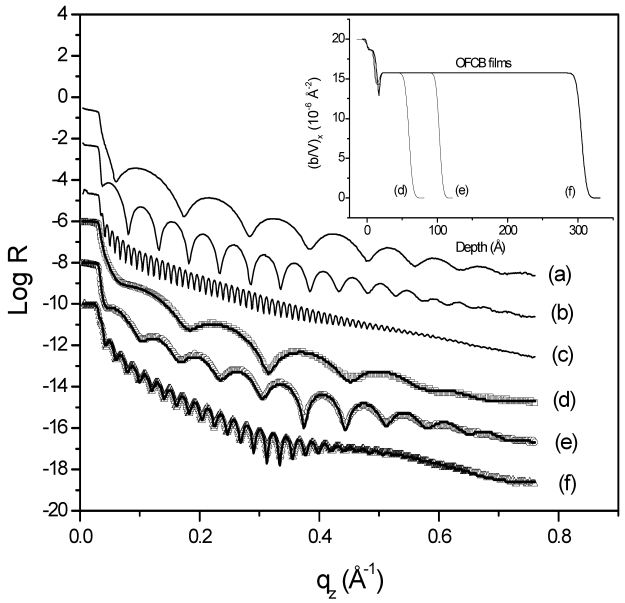

Fig. 5. Synchrotron XR data measured for six single layers, denoted by their precursor type and thickness: (a) PP-B, 67 Å, (b) PP-B, 125 Å, (c) PP-B, 652 Å, (d) PP-OFCB, 50 Å, (e) PP-OFCB, 92 Å, (f) PP-OFCB, 290 Å. For curves (a)–(c) from the PP-B films only the data are shown using solid lines. For curves (d)–(f) from the PP-OFCB films the data are shown with open symbols and solid lines superposed on the data indicate the best fits obtained with model structures shown in the inset for the corresponding films. Each data set was shifted by two orders of magnitude for clarity.

Qualitative differences between the XR curves from the PP-B samples and PP-OFCB samples can easily be observed. In the case of the PP-B films, fringes of gradually decreasing amplitude propagate to higher q_z. The XR curves for the PP-OFCB films differ from those of PP-B films in two ways. First, in each XR curve from a PP-OFCB film the first minimum after the critical edge is not as sharp as the first minima in the XR curves from the PP-B films. Secondly, the amplitude of the fringes initially gets *bigger* as q_z increases for all three PP-OFCB films, which is in good agreement with the results obtained with the rotating anode based spectrometer. Again the XR data for the PP-OFCB films cannot be fit with uniform $(b/V)_x$ models. There exists a region of lower $(b/V)_x$ immediately adjacent to the substrate for all the samples, as is shown in the inset of Fig. 5. The extents of deficiency in $(b/V)_x$ and the widths of the regions are close for the three depth profiles.

3.2. Interface structure of PP-OFCB/dB bilayer film

The structures of the PP-dB and PP-OFCB layers elucidated by measurements of the single layer films were consistent with those found in a bilayer film and a multilayer film. NR data and the best fit for a PP-OFCB/dB bilayer film are shown in Fig. 6 along with the model structure in the

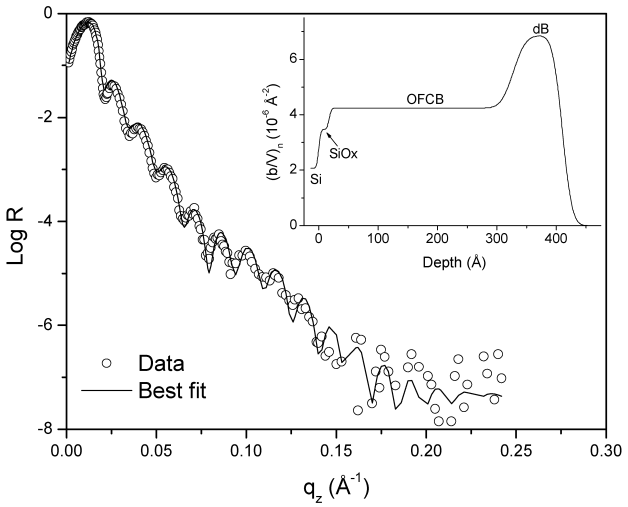

Fig. 6. NR data (open symbols) for the OFCB/dB bilayer and the best fit obtained with a model structure shown in the inset.

inset. The corresponding model parameter values obtained by both NR and XR are summarized in Table 2. We focus on the widths of the interface between layers and the interface with air. The interface between the PP-OFCB and PP-dB layers has an rms width of 16 Å, or $a_I = 40$ Å, which is about three times the widths of the film/air interfaces of the PP-dB or PP-OFCB single layer (4–5 Å rms). Feeding of the second monomer (dB) began after the first layer had formed completely. Thus, the OFCB/dB interface width might be expected to be in the same range as that of OFCB/air interface for a single layer of PP-OFCB, but instead it is broader (though still sharp by optical standards). It is highly unlikely that the interface has been broadened by interdiffusion. Both the PP-dB and PP-OFCB are reasonably tightly crosslinked. The chains or chain segments adjoining the layer/layer interface are capable of little diffusion [51]. What is not known is how much the segments at the interface may rearrange during the moments that the interface is formed by reaction. It is likely that at the same time PP-dB fragments or segments are being deposited on the PP-OFCB layer and perhaps tethered to it, elsewhere the existing PP-OFCB structure may be fragmented by the reaction. This could lead to some mixing at the interface. Presumably the degree of mixing may vary with reactivity of the activated species and thus plasma power.

The rms width of the bilayer/air interface, as measured by NR, is 13 Å. This is perhaps slightly smaller than the polymer/polymer interface width, but is decidedly larger than the air interface widths for both single layers. We return to a discussion of this width after consideration of the multilayer structure.

The interesting transition structure observed in the PP-OFCB single layer was observed also in the bilayer film in which the PP-OFCB layer was right next to the substrate. XR data for the OFCB/dB bilayer and comparisons with model reflectivities for a uniform $(b/V)_x$ model and a model with a transition region at the substrate interface are shown in Fig. 7(a). Corresponding model structure profiles are shown in Fig. 7(b). The data are presented in a slightly different way to show more clearly the difference between

Table 2
Summary of structure model parameter values for bilayer film

Layer	Parameter	PP-(OFCB/dB)	
		NR	XR
SiO_x	d (Å)[a]	18	11
Interface	σ (Å)[a]	3	2
Transition	d (Å)	NA	4
Interface	σ (Å)	NA	4
OFCB	d (Å)	310	330
Interface	σ (Å)	16	13
dB	d (Å)	83	85
Interface	σ (Å)	83	85

[a] Uncertainty in d is ±2 Å and that of σ inferred from the fitting process is 15–20%.

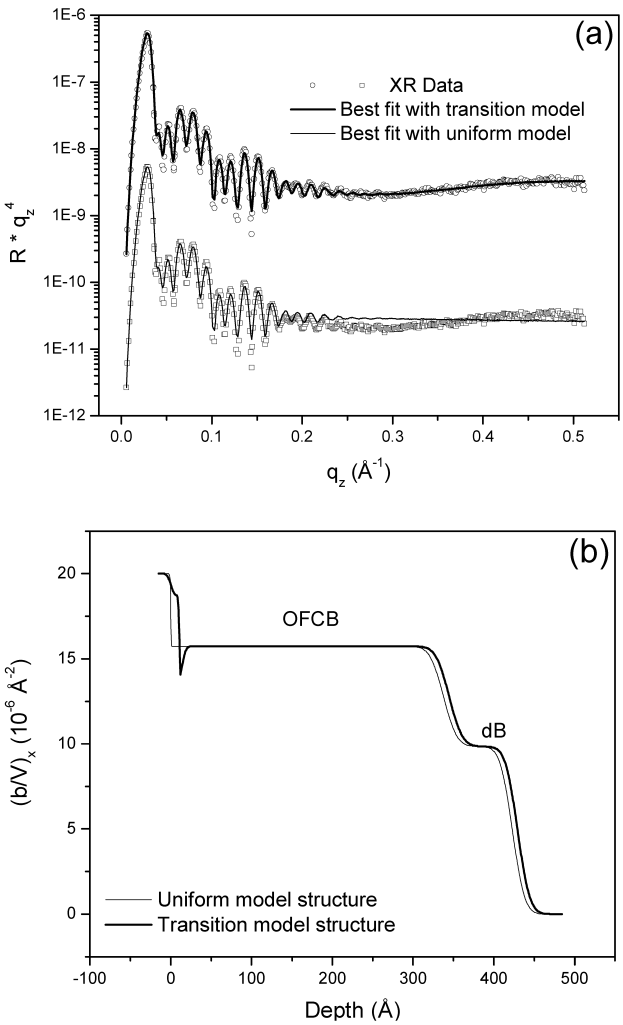

Fig. 7. Comparisons of XR data (a) measured for the OFCB/dB bilayer using the rotating anode source with simulated reflectivities from two different model structures shown in (b). Thick lines are used to show both the best fit and the corresponding model profile for the model accounting for a low density region adjacent to the substrate. Thin lines denote the best fit and corresponding model profile for the uniform density model. The XR data and the best fit obtained with the uniform model are shifted by two orders of magnitude for clarity. The uniform layer model cannot account for the fringe amplitudes for values of q_z near 0.3 Å^{-1}.

the two model reflectivities at higher q_z. The quantity plotted on the ordinate is reflectivity multiplied by q_z^4 in order to normalize for the trivial q_z^{-4} dependence seen for all interfaces at larger q_z. The quality of the best fit with the uniform $(b/V)_x$ profile model is poorer than that obtained with the transition region model. Moreover, parameter values providing the best fit for the uniform density model structure were not realistic. The model structure with uniform layer density of PP-OFCB found to fit the experimental data best did not include an SiO_x layer and the interface roughness between the Si substrate and the PP-OFCB layer was unrealistically small (1 Å rms). If the thickness and roughness of the SiO_x layer were constrained to reasonable values, we were unable to get a good fit. It has been reported [8] that SiO_x can be etched by a fluorocarbon

plasma in which highly energetic ion bombardment occurs. In that work, a transition from fluorocarbon deposition to etching of the SiO_x layer was seen to occur at around 75 W of bias power. For our study, the power input was 40 W or below and the Si substrate was placed 8–10 cm further downstream from the plasma zone. The processing condition for our samples was less severe than that for plasma etching, so it is unlikely that the SiO_x layer was etched away during the film deposition process. Furthermore, the XR data for the PP-OFCB single layer film cannot be fit with a model structure in which there is no SiO_x layer.

3.3. Interface structure of a multilayer film

The interface widths and structural uniformity in a multilayer were studied in a sample in which alternating layers of PP-dB and PP-OFCB were deposited to form five bilayers. The NR data and the best fit are shown in Fig. 8. The corresponding model parameters obtained by NR and XR are summarized in Table 3. The best fit agrees well with the measured data and the model structure shown in the inset is consistent with the results from single layer and bilayer samples. The average interface roughness between the layers is 16 ± 5 Å rms and the outer surface roughness is 8 Å rms. We conjecture that, just as with the bilayer sample, this width reflects the effects of local chemistry at the sample surface as the interface is formed.

The same quality of data fit was obtained for the XR data from the multilayer film that was used for NR measurement, as shown in Fig. 9. The average interface roughness between the layers is 15 ± 2 Å rms ($a_l = 38$ Å) and the outer surface roughness is 6 Å rms, which are in good agreement with NR results. The layer thicknesses derived from the fit of the XR data are very close to those derived from the NR data. However, one discrepancy is observed between the NR and XR data. Interface widths for the dB/OFCB interfaces derived from the X-ray data are, on average, slightly higher than those derived from neutron data. Correspondingly, interface widths for the OFCB/dB interfaces derived from the neutron data are, on average, slightly higher than those derived from the X-ray data. One possible explanation for the former observation is that there is a transition region between the PP-dB and PP-OFCB layers somewhat like the transition between SiO_x and PP-OFCB in the PP-OFCB single layer film and in the OFCB/dB bilayer film. In contrast to the case of an interface between PP-OFCB and silicon, for the layer/layer interfaces in the multilayer one does not observe a dip in the $(b/V)_x$ profile at any point. Instead, one simply observes a broadening of the interface because the $(b/V)_x$ of PP-OFCB is higher than that of PP-dB. It is not clear why neutrons see the OFCB/dB interfaces as being broader than do X-rays. We conjecture that, as with the bilayer film, layer/layer interface width inside the multilayer is the result of a combination of the intrinsic roughness of the underlying layer and the effects of

Table 3
Summary of structure model parameter values for multilayer film

Layer	Parameter	PP-5(dB/OFCB)	
		NR	XR
SiO_x	d/σ (Å)[a]	10/3	10/3
dB	d/σ (Å)	103/13	99/14
OFCB	d/σ (Å)	155/18	161/13
dB	d/σ (Å)	97/14	105/19
OFCB	d/σ (Å)	142/18	136/13
dB	d/σ (Å)	98/14	101/17
OFCB	d/σ (Å)	129/24	128/13
dB	d/σ (Å)	106/14	101/14
OFCB	d/σ (Å)	144/19	141/12
dB	d/σ (Å)	99/8	99/14
OFCB	d/σ (Å)	110/8	114/6

[a] Uncertainty in d is ± 2 Å and that of σ inferred from the fitting process is 15–20%.

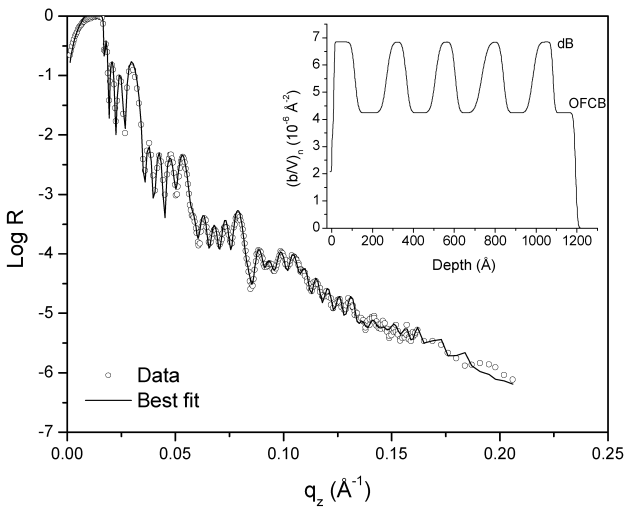

Fig. 8. NR data (open symbols) and the best fit obtained with a model structure shown in the inset for the multilayer film of PP-5(dB/OFCB).

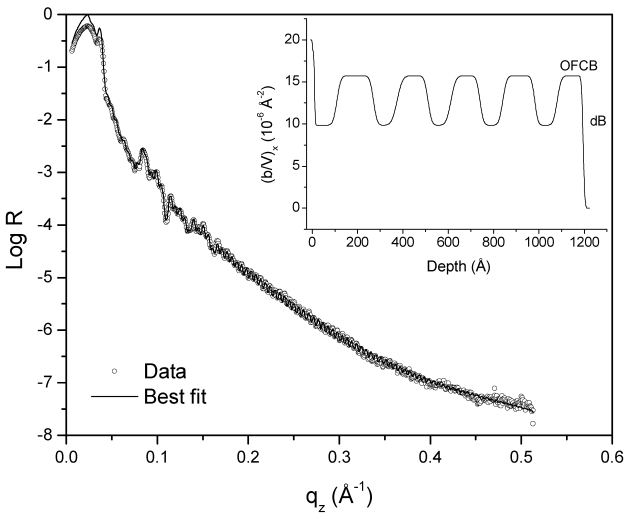

Fig. 9. XR data (open symbols) measured using Cu K_α source and the best fit obtained with a model structure shown in the inset for the multilayer film of PP-5(dB/OFCB).

simultaneous deposition of new material with some fragmentation (sputtering) of previously deposited material. The OFCB reactive species are expected to sputter more aggressively that do the dB species and this asymmetry in reactivity probably leads to differences between the dB/OFCB and OFCB/dB interfaces that are reflected in the asymmetry of the reflectivity results. The differences are sufficiently subtle that they cannot be completely resolved for this sample with measurements made over the experimentally available range of q.

The polymer/air interface roughness of the multilayer film is as low as those of the single layer films. This suggests that the higher air interface width of the bilayer does not indicate a general trend of increase in air interface width with film thickness. If the samples were liquid-like (or had been liquid-like at some point before vitrifying), the mean squared roughness at the air interfaces would be expected to increase logarithmically with the thickness of the film [52]. However, the roughnesses of the highly crosslinked PECVD films are clearly not dictated by film thickness and the surface fluctuations are strongly suppressed due to the strong confinement of the chemical bonds between the elements. Off-specular scattering that gives additional evidence of this suppression of the surface fluctuations is the subject of a separate publication [53].

4. Conclusions

Measurements of PECVD polymer films with neutron and X-ray reflectivity and self-consistent analysis of the data sets have provided an unprecedented elucidation of the interface structure created by the PECVD process. The mass densities of the PP-dB and PP-OFCB films have been obtained by analysis of the NR data from a single layer and the composition of the PP-dB film has been bounded by self-consistent analysis of all the data from single, bilayer, and multilayer films. When PP-OFCB is deposited on silicon with its native oxide, a region indicative of some transient behavior is seen at the interface. This reflects a shift in the composition of the film from the material first deposited to that in the center of the layer, but this shift is extremely rapid, as the transition region is of order 10 Å thick. The structures of single layer, bilayer and multilayer films are self-consistent. Interface widths, a_I, between layers made with different monomer are about 38 ± 5 Å (15 Å rms) based on XR and 40 ± 5 Å (16 Å rms) based on NR, while the interface formed with air when the deposition ceases is generally narrower, with an rms roughness of typically 4–8 Å. The greater width of the layer/layer interfaces is likely due to chemistry occurring locally at the deposition surface as the interface is formed. The fact that the roughness at the air interface does not increase consistently with thickness results from the strongly cross-linked nature of the material.

Acknowledgements

MDF and HK thank Bulent Akgun for help in doing experiments. MDF thanks Michael Silverstein and HK thanks Takao Usami for their helpful discussions. This research was funded by the Collaborative Center for Polymer Photonics (F49620-02-1-0428). Use of the Advanced Photon Source was supported by the US Department of Energy, Office of Science, Office of Basic Energy Science, under Contract No. W-31-109-ENG-38.

References

[1] Martinu L, Poitras D. J Vac Sci Technol, A 2000;18(6):2619.
[2] Yasuda H. Plasma polymerization. Orlando: Academic Press; 1985.
[3] Sandrin L, Silverstein MS, Sacher E. Polymer 2001;42(8):3761.
[4] Silverstein MS, Sandrin L, Sacher E. Polymer 2001;42(9):4299.
[5] Takahashi K, Tachibana K. J Appl Phys 2001;89(2):893.
[6] Jobanputra MC, Durstock MF, Clarson SJ. J Appl Polym Sci 2003;87(3):523.
[7] Yase K, Horiuchi S, Kyotani M, Yamamoto K, Yaguchi A, Futaesaku Y, Suwa T, Kakimoto M-A, Imai Y. Jpn J Appl Phys, Part 2 1996;35(5B):L657.
[8] Schaepkens M, Oehrlein GS. J Electrochem Soc 2001;148(3):C211.
[9] Weber A, Pöckelmann R, Klages CP. J Vac Sci Technol, A 1998;16(4):2120.
[10] Labelle CB, Gleason KK. J Vac Sci Technol, A 1999;17(2):445.
[11] Kim KJ, Lee NE, Kim MC, Boo JH. Thin Solid Films 2001;398–399:657.
[12] Valentini L, Kenny JM, Montereali RM, Lozzi L, Santucci S. Mat Sci Semicon Proc 2003;5(2–3):271.
[13] Shirafuji T, Miyazaki Y, Hayashi Y, Nishino S. Plasmas Polym 1999;4(1):57.
[14] Jiang H, Johnson WE, Grant JT, Eyink K, Johnson EM, Tomlin DW, Bunning TJ. Chem Mater 2003;15(1):340.
[15] Cho SH, Park ZT, Kim JG, Boo JH. Surf Coat Technol 2003;174–175:1111.
[16] Alexandrova S, Danesh P, Maslyanitsyn IA. Vacuum 2003;69(1–3):391.
[17] Sun Z. J Non-Cryst Solids 2000;261(1–3):211.
[18] Sassella A, Lucarno P, Borghesi A, Corni F, Rojas S, Zanotti L. J Non-Cryst Solids 1995;187:395.
[19] Gottschalch V, Schmidt R, Rheinländer B, Pudis D, Hardt S, Kvietkova J, Wagner G, Franzheld R. Thin Solid Films 2002;416(1–2):224.
[20] Zhang Z, Chen Q, Knoll W, Foerch R, Holcomb R, Roitman D. Macromolecules 2003;36(20):7689.
[21] Anastasiadis SH, Russell TP, Satija SK, Majkrzak CF. Phys Rev Lett 1989;62(16):1852.
[22] Torikai N, Noda I, Karim A, Satija SK, Han CC, Matsushita Y, Kawakatsu T. Macromolecules 1997;30(10):2907.
[23] Anastasiadis SH, Retsos H, Toprakcioglu C, Menelle A, Hadziioannou G. Macromolecules 1998;31(19):6600.
[24] Foster MD, Sikka M, Singh N, Bates FS, Satija SK, Majkrzak CF. J Chem Phys 1992;96(11):8605.
[25] Russell TP, Menelle A, Hamilton WA, Smith GS, Satija SK, Majkrzak CF. Macromolecules 1991;24(20):5721.
[26] Freitas Siqueira D, Schubert DW, Erb V, Stamm M, Amato JP. Colloid Polym Sci 1995;273(11):1041.
[27] Sferrazza M, Xiao C, Jones RAL, Bucknall DG, Webster J, Penfold J. Phys Rev Lett 1997;78(19):3693.
[28] Genzer J, Composto RJ. Polymer 1999;40(15):4223.
[29] Hayashi M, Hashimoto T, Hasegawa H, Takenaka M, Grüll H, Esker

AR, Weber M, Satija SK, Han CC, Nagao M. Macromolecules 2000; 33(22):8375.
[30] Anastasiadis SH, Russell TP, Satija SK, Majkrzak CF. J Chem Phys 1990;92(9):5677.
[31] Johnson JA, Woodford JB, Erdemir A, Fenske GR. Appl Phys Lett 2003;83(3):452.
[32] Bontempi E, Depero LE, Sangaletti L, Giorgis F, Pirri CF. Mater Chem Phys 2000;66(2–3):172.
[33] Ermolieff A, Chabli A, Pierre F, Rolland G, Rouchon D, Vannuffel C, Vergnaud C, Baylet J, Semeria MN. Surf Interface Anal 2001;31(3): 185.
[34] Yim H, Kent MS, Matheson A, Stevens MJ, Ivkov R, Satija S, Majewski J, Smith GS. Macromolecules 2002;35(26):9737.
[35] Kügler R, Knoll W. Macromol Chem Phys 2002;203(7):923.
[36] Mouri E, Matsuoka H, Kago K, Yoshitome R, Yamaoka H, Tasaki S. Stud Surf Sci Catal 2001;132:439.
[37] Foster MD. Crit Rev Anal Chem 1993;24(3):179.
[38] Liebmann-Vinson A, Lander LM, Foster MD, Brittain WJ, Vogler EA, Majkrzak CF, Satija S. Langmuir 1996;12(9):2256.
[39] Petrash S, Liebmann-Vinson A, Foster MD, Lander LM, Brittain WJ, Majkrzak CF. Biotechnol Prog 1997;13(5):635.
[40] Zhao W, Zhao X, Rafailovich MH, Sokolov J, Mansfield T, Stein RS, Composto RC, Kramer EJ, Jones RAL, et al. Physica B: Condens Matter 1991;173(1–2):43.
[41] Haaland P, Targove J. Appl Phys Lett 1992;61(1):34.
[42] Commercial materials, instruments, and equipment are identified in this paper in order to specify the experimental procedure as completely as possible. In no case does such identification imply a recommendation or endorsement by the National Institute of Standards and Technology nor does it imply that the materials, instruments, or equipment identified are necessarily the best available for the purpose.
[43] Russell TP. Mater Sci Rep 1990;5(4–5):171.
[44] Vierheller TR. Interfacial microstructure and dynamics in Langmuir–Blodgett multilayer thin films containing cadmium arachidate and polyglutamate copolymers. PhD Thesis. The University of Akron; 1994.
[45] Sheller NB, Petrash S, Foster MD, Tsukruk VV. Langmuir 1998; 14(16):4535.
[46] Lang JC, Srajer G, Wang J, Lee PL. Rev Sci Instrum 1999;70(12): 4457.
[47] Parratt LG. Phys Rev 1954;95:359.
[48] Schalchli A, Benattar JJ, Licoppe C. Europhys Lett 1994;26(4):271.
[49] Toney MF, Brennan S. J Appl Phys 1989;66(4):1861.
[50] Morrison RT, Boyd RN. Organic chemistry, 5th ed. Newton: Allyn and Bacon; 1987.
[51] Maeda N, Chen N, Tirrell M, Israelachvili JN. Science 2002; 297(5580):379.
[52] Tolan M. X-ray scattering from soft-matter thin films. New York: Springer; 1999.
[53] Kim H, Foster MD, Jiang H, Tullis S, Bunning T, Wang J. In preparation.